Usak University Journal of Material Sciences
journal homepage: http://yayinlar.usak.edu.tr/uujms

Research article

Insitu Synthesis and Characterization of Mullite-Carbon Refractory Ceramic Composite from Okpella Kaolin and Graphite

Fatai Olufemi Aramide [a,b], Idris Babatunde Akintunde[a], Akinlabi Oyetunji[ac]*

[a]*Department of Metallurgical and Materials Engineering, Federal University of Technology, P.M.B. 704, Akure, Nigeria*

[b]*African Materials Science and Engineering Network, (AMSEN) a Subsidiary of Regional Initiative for Science Education (RISE)*

Abstract

Mullite fibres were developed within the carbon matrix through high temperature reaction sintering of kaolinite to produce mullite-carbon refractory ceramic composite. The effects of sintering temperatures on the phases developed and the physico-mechanical properties of the mullite-carbon refractory ceramic composite produced was investigated. The kaolin clay was sourced from Okpella, Edo State, Nigeria. The raw kaolin and graphite were prepared for characterization, to determine their mineralogical phases. Kaolin was thoroughly blended with 40 vol. % graphite in a ball mill. The test samples that contain homogeneous mixture of kaolin and graphite were produced via uniaxial compaction. The compacted samples were subjected to firing (sintering) at 1300˚C, 1400˚C and 1500˚C held at the temperature for an hour. The sintered samples were then characterized for the developed phases using x-ray diffractometry analysis, microstructural morphology using ultra-high resolution field emission scanning electron microscope, various physical and mechanical properties were determined. The results obtained from microstructural morphology of the samples revealed the evolution of mullite, that turns needle-like shaped fibre as the temperature was raised to 1500°C. Other phases synthesized in the samples were cristobalite and microcline. The mineralogical phase of the samples revealed the increments in the evolution of mullite and also the variation in other phase attained as the sintering temperature was raised from 1300°C to 1500°C for the sample having the same composition. It was concluded that sample with optimum physico-mechanical properties is obtained at 1400°C.

Keywords: *kaolin; mullite; graphite (carbon); sintering temperatures; phase transformation; sintered ceramic composite.*

1. Introduction

There is an increasing interest in ceramic materials with improved high temperature mechanical behaviour for structural applications. Recently, materials production and utilization has shifted from monolithic to composite materials, adjusting to the global need for reduced weight, low cost, quality, and high performance in structural materials [Aramide, (2015); Aramide *et al.* (2014)]. This lead to high consumption in the utilization

*Corresponding author:
E-mail: foaramide@futa.edu.ng
DOI: 10.12748/uujms.2017.39

of CMCs in areas such asiron and steel industry, refinery, chemical, hardware, cement and glass industries that include: performance, economic and environmental benefits. The well acknowledged good performance in service and consequent high demand for mullite-carbon ceramic composite is attributed to its excellent combination of properties such as mechanical,thermal and chemical properties [Aneziris *et al.* (2007); Lee and Zhang, (2004); Aneziris *et al.* (2003)].

Mullite produced from cheap and abundantly available natural raw materials such as kaolin is preferred to produce refractory-grade aggregates that are techno-economically viable for bulk refractory applications. Reaction sintering of Al_2O_3 and SiO_2 bearing materials is a low cost method of mullite formation [Tripathi *et al.* (2001)]. The temperature and rate of mullite formation depends on the starting material, their chemical purity and particle size. Typically Al_2O_3 and SiO_2 containing reactants used for this purpose are clay minerals such as kaolinite, pyrophyllite, sillimanite group of minerals and bauxite [Viswabaskaran *et al.* (2003)].

Like mullite-zirconia which have been widely used for high-temperature applications for their different superior physico-mechanical properties [Temoche *et al.* (2005)]. Mullite-carboncomposites will compete with the existingmullite-zirconia in its area of applications. For the preparation of zirconia-mullite composites, reaction sintering route has gained much attention due to the availability of the starting materials and the lower processing temperature required. Many works have been reported on the reaction sintering of zirconia-mullite composites and some of these are mentioned below. Das and Banerjee, (2000) prepared reaction sintered zirconia-mullite composites using zircon flour, alumina and dysprosia as sintering additive. Rendtorff*et al*. (2008) used two different processing routes: for the preparation of zirconia-mullite composites, which are reaction sintering of alumina and zircon and direct sintering of mullite-zirconia grains by slip casting and sintered at 1600˚C for 2 hours. Ozturk and Tur, (2007) prepared textured mullite-zirconia composites preparation from a reactive mixture of alumina and zircon powders together with acicular aluminum borate templates to nucleate and texture mullite grains in the [001]. Badiee *et al.* (2001) studied the effect of CaO, MgO, TiO_2, and ZrO_2on mullitization of the Iranian andalusite located in Hamedan mines. They found out that the first three of these additives encouraged mullite formation from andalusite.
Ebadzadeh and Ghasemi (2002) prepared zirconia-mullite composites using α-alumina and aluminium nitrate and zircon powder with TiO_2 as additive. Aramide *et al.* (2014) synthesized mullite-zirconia composites containing yttria as additive. Chandra*et al.* (2013) prepared zirconia-toughened ceramics with a mullite matrix based on the quaternary system ZrO_2-Al_2O_3-SiO_2-TiO_2 in the temperature range 1450-1550˚C using zircon-alumina-titania mixtures. Aksel and Komicezny (2001) studied the influence of zircon on the mechanical properties and thermal shock behaviour of slip-cast alumina-mullite refractories.

The objective of the present study is to explore the utilization of kaolin and graphite to synthesize mullite-carbon ceramic composite. This area of research is becoming very important in a good number of developing countries where there are sustained efforts to develop better materials (refractories) to withstand high temperature through the adoption of indigenous materials and technologies.

2. Materials and Methods

2.1. Raw Materials

Clay sample used for this study (as mine Kaolin sample) was sourced from Okpella, Edo State southern part of Nigeria andSpent Graphite Electrode (SGE) was sourced from (Pascal Chemicals, Akure), this were used to maintain the granulometry of the mixture.

2.2. Method

2.2.1. Processing of raw materials (Graphite Electrode and Kaolin)

The raw materials (Spent graphite electrode and kaolin) were crushed into a coarse particle size, of about 10 mm for graphite and less than 2mm for kaolin; the crushed samples were further reduced by grinding using Herzog rod mill. The powdered samples were sieved using 600μm sizes aperture according to ASTM standards in an electric sieve shaker. The undersize that passed through the 600μm sieve aperture were used in the samples making.

2.2.2. Phase and Mineralogical Composition of Raw kaolin and Graphite Electrode

The kaolin clay and graphite electrode samples were carefully prepared for these analyses by digesting in reagents as described by Nabil and Barbara, (2012). The mineralogical phases present in the samples were determined using X-ray diffractometry (XRD). The phases are reported in Figures 1 and 2 and also in Table 1.

2.3. Experimental Procedure

2.3.1. Composition calculation using the Rule of Mixtures Technique

Rule of Mixtures is a method of approach to approximate estimation of composite material properties, based on an assumption that a composite property is the volume weighed average of the phases (matrix and dispersed phase). According to Rule of Mixtures [Surappa, (2003)] the density of composite materials are estimated as follows:

$$\rho_{mixture} = WF_K \times \rho_K \times WF_g \times \rho_g \quad (1)$$

$$M_{mixture} = \rho_{mixture} \times V_{mould} \quad (2)$$

Where: $\rho_{mixture}$ represent density of the mixture, $M_{mixture}$ is the mass of the mixture, WF_K is the weight fraction of kaolin, ρ_K is the density of kaolin, WF_g is the weight fraction of graphite, ρ_g is the density of graphiteand V_{mould} is volume of mould.

2.3.2. Composites Production

The raw materials in the samples making were 60:40vol. % of kaolin and graphite respectively. The mixture were blended thoroughly for proper distribution of constituents materials in a ball mill for 3 hours at a speed of 72 rev/min after weighing via electronic weighing balance in accordance with the composition calculation initially prepared [Aramide, (2015); Aramide *et al.* (2014)]. After which the resulting blended compositions were mixed with water, the water added was 10% the amount of kaolin content in each composition, this was in order to enhance the plasticity of the mixture during compaction. The mixed samples were subjected to uniaxial compaction, which

was carried out mechanically under pressure. The moulded materials were fired at varying temperatures (1300˚C, 1400˚C and 1500˚C). After which the samples were subjected to various test, to examine the phase analysis, evaluate their physical and mechanical properties.

2.4. Testing

2.4.1. Shrinkage Measurement

The shrinkage properties of the pressed samples were determined by measuring both the green and fired dimensions, using a digital vernier caliper. The thickness and diameters were measured for evaluation and computation of the shrinkage [Aramide, (2015)].

$$\% \text{ linear shrinkage } = \frac{(\text{Lg}-\text{Lf})}{(\text{Lg})} \times 100 \quad (3)$$

where: Lg represent the green length and Lf represent the fired length.

$$\% \text{ volumetric shrinkage } = \frac{(\text{Vg}-\text{Vf})}{(\text{Vg})} \text{ x } 100 \quad (4)$$

where: Vg represent the green volume and Vf represent the fired Volume

2.4.2. Apparent porosity (AP)

Test samples from each of the ceramic composite samples were dried out for 12 hours at 110˚C. The dry weight of each fired sample was taken and recorded as D. Each sample was immersed in water for 6 hours to soak and weighed while being suspended in air. The weight was recorded as W. Finally, the specimen was weighed when immersed in water [Aramide, (2015); Aramide *et al.* (2014)]. This was recorded as S. The apparent porosity was then calculated from the expression:

$$\% \text{ apparent porosity} = \frac{(\text{W}-\text{D})}{(\text{W}-\text{S})} \text{ x } 100 \quad (5)$$

2.4.3. Bulk Density

The test specimens were dried out at 110˚C for 12 hours to ensure total water loss. Their dry weights were measured and recorded. They were allowed to cool and then immersed in a beaker of water. Bubbles were observed as the pores in the specimens were filled with water. Their soaked weights were measured and recorded. They were then suspended in a beaker one after the other using a sling and their respective suspended weights were measured and recorded [Aramide, (2015); Aramide *et al.* (2014)]. Bulk densities of the samples were calculated using the formula below:

$$\text{Bulk density} = \frac{\text{D}}{(\text{W}-\text{S})} \quad (6)$$

where: D represents weight of dried specimen, S represents weight of dried specimen suspended in water, and W represents weight of soaked specimen suspended in air.

2.4.4. Water Absorption

The test sample was dried out in an oven till a constant weight of the sample was obtained. The sample was then placed in a vessel containing water in order to be completely submerged without touching the bottom of the vessel in which it is suspended. The vessel was then heated slowly so that the water boiled after heating. After boiling for about an hour with the evaporated water replaced, the sample was allowed to cool at room temperature for 24 hours. The sample was then renamed, blotted and then reweighed [Aramide, (2015)]. The percentage water absorption was calculated as showed below:

$$\%\text{water absorption} = \frac{(\text{soaked wt} - \text{dried wt})}{(\text{dried wt})} \quad (7)$$

2.4.5. Cold Compression Strength, Modulus of Elasticity and Absorbed Energy

Cold compression strength test is to determine the compression strength to failure of each sample, an indication of its probable performance under load. The standard ceramic samples were dried in an oven at a temperature of 110˚C, allowed to cool. The cold compression strength tests were performed on INSTRON 1195 at a fixed crosshead speed of 10mm min-1. Samples were prepared according to ASTM C133-97 (ASTM C133-97, 2003) [Aramide, (2015); Aramide *et al.* (2014)] cold crushing strength, modulus of elasticity and absorbed energy of standard and conditioned samples were calculated from the equation:

$$\text{CCS} = \frac{(\text{Load to fracture})}{(\text{Surface area of sample})} \quad (8)$$

2.4.6. Oxidation Resistance

The fired samples after heat-treatment were cut and the diameter of black portion was measured at different locations and the average value was taken. Lower oxidation index indicates the higher oxidation resistance of the sample [Singh, (2014); Mahato, (2013)]. Oxidation index is determined by the formula:

$$\text{Oxidation index} = \frac{(\text{Area of oxidized zone}}{\text{Total area)}} \times 100 \quad (9)$$

3. Results and discussion

3.1. Phase/Mineralogical Composition of the Raw Kaolin and Graphite Samples

The phase/mineralogical composition of the kaolin and graphite samples were characterised (investigated) with the aid of X-ray diffractometer. The results of the phase analysis of kaolin and graphite powder quantified by XRD were presented in Table 1.

The XRD phase/mineralogical composition of preliminary tests made on the kaolin and graphite powdered samples show the quality and quantity of different phases present in weight percent. Table 1 shows the X-ray diffraction results of kaolin and graphite powder samples. The major mineral phase of kaolin identified is kaolinite 63.2%, small amount of quartz 0.6% is also detected by the analysis. Furthermore, 36.1% amorphous phase is also detected. The amorphous phases are the non-crystalline contents of the samples; since xrd can only identify crystalline components. According to Chen *et al.* (2000) the

XRD pattern of Malaysian kaolin powder sample shows apart from kaolinite phase, a small amount of quartz and muscovite (mica) were also detected by the analysis. Benea and Gorea, (2004) reported that KOI and MK2 kaolin samples from Ukraine and BOJ kaolin sample from Bulgaria contain the following mineral phases as identified by XRD analysis. KOI contains; 89 wt.% kaolinite, 6 wt.% illite and 5 wt.% quartz, MK2 contains; 69.85 wt.% kaolinite, 19.5 wt.% illite, 7.6 5 wt.% quartz and 3 wt.% vermiculite. BOJ contains; 82.95 wt.% kaolinite, 10.4 wt.% illite and 6.65 wt.% quartz. Due to relatively high amount of quartz and vermiculite, MK2 shows a weak rheology while BOJ kaolin type is the most suitable raw material for ceramic casting bodies due to high plasticity and drying resistance, low drying shrinkage and good rheology. According to Hamisi *et al.* (2014) the mineralogical phase of Pugu kaolin hills deposits approximately 25 km south-south-west of Dar-es Salaam and 20 km inland from the Indian Ocean contain mainly of kaolinite. Brasileiro *et al.* (2012) reported that the kaolin obtained from Borborema pegmatitic plain, located in the municipality of Juazeirinho-Paraíba - Brazil contain kaolinite, quartz and mica. According to Mesbah *et al.* (2010) the phase composition of kaolin, supplied by Fisher Scientific Ltd, UK, contain majorly of kaolinite.

From the above, Okpella kaolin sample like MK2 and BOJ reported to be suitable for ceramic application. It is observed that Okpella kaolin contains extremely lower amount of quartz as compare to BOJ and MK2 which make it suitable for the production of refractory and other ceramic applications at elevated temperature due to little or no liquid glass phase formation that lead to more pores in the ceramic material produced. It will also find application in paint and pharmaceutical industry.

Table 1
XRD Results of kaolin and graphite sample showing the quantity of different phases present

Materials	Kaolinite (wt. %)	Quartz (wt. %)	Amorphous (wt. %)	Graphite (wt. %)
Kaolin Sample	63.23	0.65	36.13	-
Graphite Sample	-	-	56.9	43.1

3.2. Effects of Sintering Temperature on the Phase Development, Physical and Mechanical Properties of Mullite-Carbon Ceramic Composite Samples Produced from Raw Kaolin and Graphite

3.2.1. Effects of Sintering Temperature on the Phase Development in the Mullite-Carbon Ceramic Composite Samples Produced from Raw Kaolin and Graphite

The XRD results of the sintered ceramic composite samples are presented in Table 2; it summarizes the quantity of phase present in the samples sintered at various temperature.

The XRD analysis, show that the sintered samples contains mullite, graphite, amorphous, cristobalite and microcline phases while Fig. 1 show the SEM morphology of the phase present in the sample. It is observed that with an increase in sintering temperature, mullite phase increased rapidly from 1300°C to 1500°C, also there is an increase in the cristobalite phase from 1300˚C to 1500°C. Microcline reduced from 1300°C to 1400°C and increased beyond the value attained at 1300°C when the temperature was raised to 1500°C. The graphite and amorphous reduced from 1300°C to 1500°C. According to Chen *et al*. (2000) mullite phase first appears at a temperature.

Table 2
Phase developed in the sintered ceramic Sample at various temperature

Sample A	Phase developed in the samples at various temperature				
Temperature (˚C)	**Graphite (wt. %)**	**Cristobalite (wt. %)**	**Mullite (wt. %)**	**Microcline (wt. %)**	**Amorphous (wt. %)**
1300	21.54	2.06	55.94	0.92	19.55
1400	20.77	6.17	56.95	0.75	15.37
1500	20.7	7.1	64.31	0.97	6.92

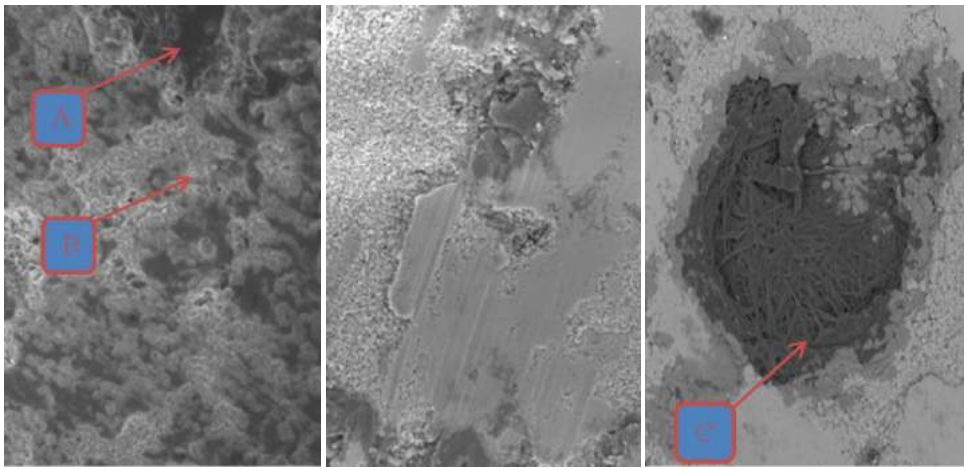

(a) (b) (c)

Fig.1 Typical SEM micrographs (Back Scattered Image) of the Sample showing its morphology at varied temperature; (a)Sample at 1300˚C showing the Secondary Electron Image A= graphite phase and B= mullite phase, (b)Sample at 1400˚C showing theSecondary Electron Image of graphite phase and mullite phase, (c)Sample at 1500˚C showing the Secondary Electron Image of graphite phase and C= mullite fibre Phase.

around 1100°C, its amount increases with increase in temperature. Furthermore, according to the reports of other researchers [Aramide, (2012); Aramide and Seidu, (2013); Qiu *et al.* (2004); Gualtieri, (2007); McConville and Lee, (2005)], the dehydration of kaolinite completes by ~150°C, followed by dehydroxylation at ~420-660°C and its structural breakdown occurs in the temperature range ~800-900°C, depending upon the particle size and amount and type of the impurities present. From Table 2, Okpella kaolin contains 63.23% kaolinite, 0.65% quartz, 36.13% amorphous that undergo a series of phase transformation as the temperature was raised from 1300-1500°C, the sintering reactions take place via;

$$Si_2Al_2O_5(OH)_4 \xrightarrow{\sim 420\text{-}660^{\circ}C} Al_2O_3{\cdot}2SiO_2 + 2H_2O$$

which involves the combination of two OH groups to form H2O and oxygen which remains incorporated in metakaolin. At about 900˚C, metakaolinite decomposes to amorphous SiO2and γ-Al2O3–type spinel via

$$Al_2O_3{\cdot}2SiO_2 \xrightarrow{900^{\circ}C} \gamma\text{-}Al_2O_3+2SiO_2$$

γAl_2O_3-type spinel and SiO_2 recrystallize into mullite at temperatures above 1100˚C via

$$3\gamma\text{-}Al_2O_3+2SiO_2 \xrightarrow{>1100^{\circ}C} 3Al_2O_3{\cdot}2SiO_2$$

Srikrishna, *et al.* (1990), reported the formation of a single phase (with composition close to mullite) and excess SiO2 at 900°C. Thus the formation of mullite begins at temperatures >900°C and the process continues till 1000°C. The increase recorded in the amount of cristobalite resulted from more silica formed during transformation of metakaolin toaluminium-silicon spinel at 925°C-950°C and also as a result of crystalline cristobalite formed along with platelet mullite during spinel transformation at 1050°C. Furthermore, the diminishing in graphite content due to increase sintering temperature was observed. [Sadrnezhaad *et al.* (2006); Sadrnezhaad *et al.* (2007); Nemati *et al.* (2005)] reported that high temperature oxidation of graphite leads to drastic deterioration in the microstructure due to graphite diminution.

3.2.2. Effects of Sintering Temperature on the Physical and Mechanical properties of Mullite-Carbon Ceramic Composite Samples Produced from Raw Kaolin and Graphite

Evaluation of the effect of sintering temperature on various physical and mechanical properties of sample A ceramic composite are presented below.

3.2.2.1. Apparent Porosity (AP)

The effect of sintering temperature on apparent porosity of the sample is vividly shown in Table 3 and Fig. 2. From the Figure, it is observed that the apparent porosity of sample A at 1300˚C is 29.5%, as the sintering temperature was increased to 1400˚C the AP slightly reduced to 29.19%, further increase in the sintering temperature to 1500˚C leads to slight increment in the apparent porosity of the sample to 29.93%. This implies that the densification of the sample continues from 1300˚C to 1400˚C due to the sintering process. According to Calister, (2007) voids exist between particles of the newly formed green (unfired) ceramic, much of these inter-particles voids are eliminated during firing/sintering to produce sintered ceramic. Furthermore, according to [Aramide *et al.* (2014); Aramide, (2012); Brasileiro *et al.* (2006)] the decrease in the value of AP from 1300˚C to 1400˚C is because of additional increase in the filling of spaces between bigger particles contained in the ceramic samples. The drastic increase in apparent porosity from 1400˚C to 1500˚C is as a result of carbon reaction with oxygen, the carbon burnt off, leaving pores within the samples. According to some other researchers, [Sadrnezhaad *et al.* (2006); Sadrnezhaad *et al*. (2007); Nemati *et al.* (2005)] high temperature oxidations of graphite lead to drastic deterioration due to graphite diminution, which result to pores in the samples.

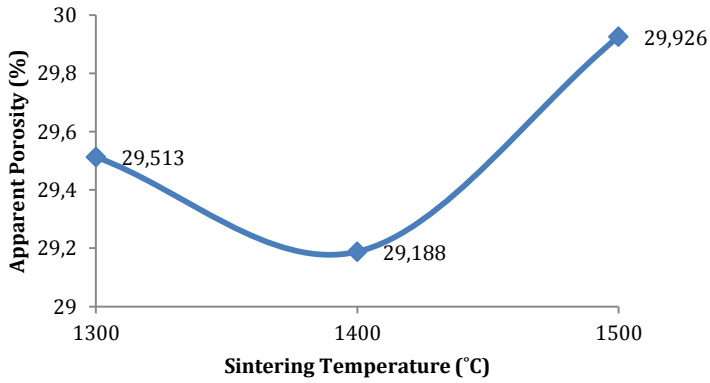

Fig. 2 Effects of Sintering Temperature on the Apparent Porosity of the Sample

3.2.2.2. Bulk Density

The effect of sintering temperature on bulk density of the sample is clearly shown in Table 3 and Fig. 3. From the Figure, it is observed that the bulk density of the sintered ceramic sample is low, the value ranges from 1.47 g/cm^3 to 1.71 g/cm^3. The bulk density of the sintered sample at 1300˚C is 1.60 g/cm^3, with an increase in temperature to 1400˚C, the bulk density increases to 1.71 g/cm^3. However, further increase in sintering temperature to 1500˚C, the bulk density of the sample reduces to 1.47 g/cm^3 this is as dictated by the apparent porosity. The increase in bulk density from 1300˚C to 1400˚C is due to densification of the sample, further firing the sample at high temperature burn off some amount of carbon leading to increased porosity as a result of reduced matter contents of the samples as seen at 1500˚C. According to Chen *et al.* (2000) the apparent density does not show significant difference in relation to the compositions and sintering densification in this range of temperature (1300˚C-1500˚C) which make the BD to be relatively low and suggests the formation of secondary mullite from the reaction between vitreous phase and alumina. Furthermore, according to [Aramide, (2012); Brasileiro *et al.* (2006)] the increase in bulk density from 1300˚C to 1400˚C is because of additional increase in the filling of spaces between bigger particles contained in the ceramic samples.

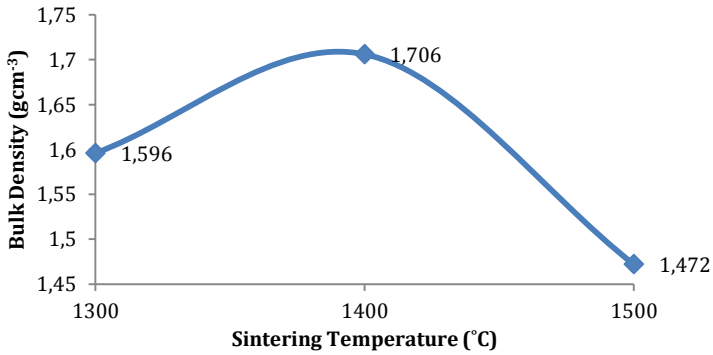

Fig. 3 Effects of Sintering Temperature on the Bulk Density of the Sample.

3.2.2.3. Water Absorption

The effect of sintering temperature on water absorption of the sample is clearly shown in Fig. 4. From the Figure, it is observed that the water absorption of the sintered ceramic sample is 19.069% at 1300˚C, with an increase in temperature to 1400˚C, the water absorption reduced to 18.75%. However, further increase in sintering temperature to 1500˚C, the water absorption of the sample increased to 20.204%. This followed the trend recorded for apparent porosity, which implies that the water absortion of the sample reduced when the sintering temperature was increased from 1300˚C to 1400˚C, the water absorption later increased when the sintering temperature was raised to 1500˚C. This is because firing thesample at high temperature burn off some amount of carbon leading to increased porosity as a result of reduced matter contents of the samples. This is due to the sintering process; according to Calister, (2007) voids exist between particles of the newly formed green (unfired) ceramic, much of these inter-particles voids are eliminated during firing/sintering to produce sintered ceramic.

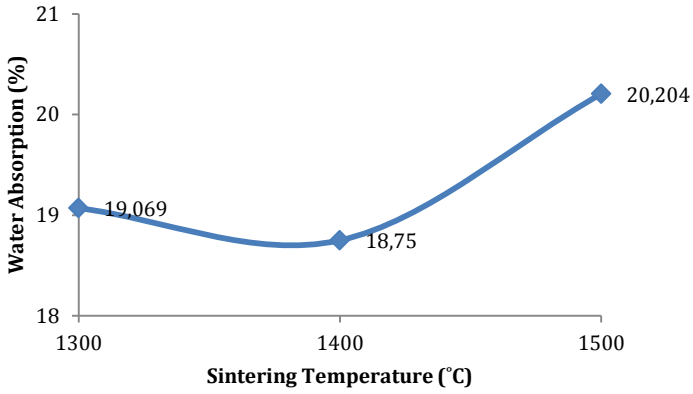

Fig. 4 Effects of Sintering Temperature on the Water Absorption of the Sample.

3.2.2.4. Cold Crushing Strength (CCS)

The effect of sintering temperature on the cold crushing strength of sample A is shown in Fig. 5 and Table 3. From the Figure, it is observed that the CCS of sample A at 1300˚C is 7.23Mpa, 8.05Mpa at 1400˚C and 7.01Mpa at 1500˚C. This indicate that with an increase in the sintering temperature from 1300˚C to 1400˚C, the cold crushing strength increases, the CCS reduced below the CCS of 1300˚C when the sintering temperature was raised to 1500˚C. The results, as dictated by bulk density which was dictated by the porosity level of the sample. The reason for this is that an increase in the bulk density of the sample, means thatthe sample contains more matter to bear the applied load [25-26]. Furthermore, according to Brasileiro *et al.* (2006), increase in CCS may be assigned to better filling of pores, higher Bulk density and the increase amount of mullite that improve on the mechanical properties. Ebadzadeh, (2005) reported that the factors that affect the mechanical properties is are the high porosity and the big size of the mullite grain.

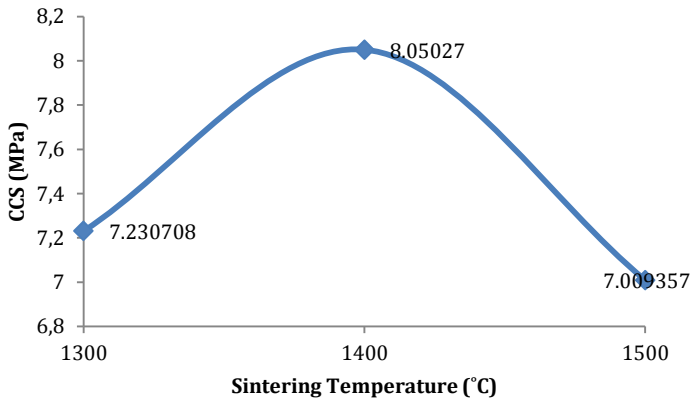

Fig. 5 Effects of Sintering Temperature on the CCS of the Sample

3.2.2.5. Modulus of Elasticity (MOE)

The effect of sintering temperature on the modulus of elasticity (MOE) of the sample is shown in Fig. 6 and Table 3. From the Figure, the MOE value of sample A at 1300˚C is 122.456 Mpa, 141.28 Mpa at 1400˚C and 86.004 Mpa at 1500˚C. This implies that with an increase in sintering temperature, the modulus of elasticity significantly increased from 1300˚C to 1400˚C, further increase in sintering temperature to 1500˚C, the MOE significantly reduced. The observed variation recorded for MOE follows the same trend with that observed for the cold crushing strength as earlier discussed.

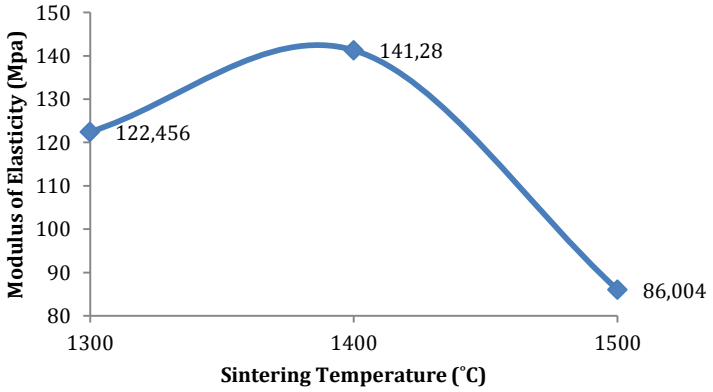

Fig. 6 Effects of Sintering Temperature on Modulus of Elasticity of the Sample

3.2.2.6. Absorbed Energy (AE)

The effect of sintering temperature on the absorbed energy (AE) of the sample is shown in Fig. 7 and Table 3. From the Figure, it is observed that the absorbed energy of sample A at 1300˚C is 3.66J, with an increase in temperature to1400˚C, the absorbed energy increased to 6.41J. However, further increase in the sintering temperature to 1500˚C, the absorbed energy of the sample reduces to 4.21J. The observed variation of the

absorbedenergy with increased sintering temperature follows the same trend with that observed for the cold crushing strength discussed earlier.

3.2.2.7. Linear expansion (LE)

The effect of sintering temperature on the linear expansion (LE) is shown in Fig. 8 and Table 3. From the Figure, it is observed that the linear expansion of the sample at 1300˚C is 1.16%, with an increase in sintering temperature, to 1400˚C the LE decreases to 0.22%. Further increase in the sintering temperature to 1500˚C the linear expansion increases to 0.76%. The sample is observed to expand, due to graphite presence in the sample. The linear expansion of the samples reduced as graphite content reduces from 1300˚C to 1500˚C, the increases in linear expansion recorded from 1400˚C to 1500˚C is due to further increase in sintering temperature. The shrinkage due to cristobalite and mullite transformation was first compensated by the graphite expansion before the sample later expand. Graphite has 0.6-4.3×10^{-6}m/mk^{-1} as coefficient of linear expansion, the expansion was clearly recorded as an increment in the length of the samples after sintering.

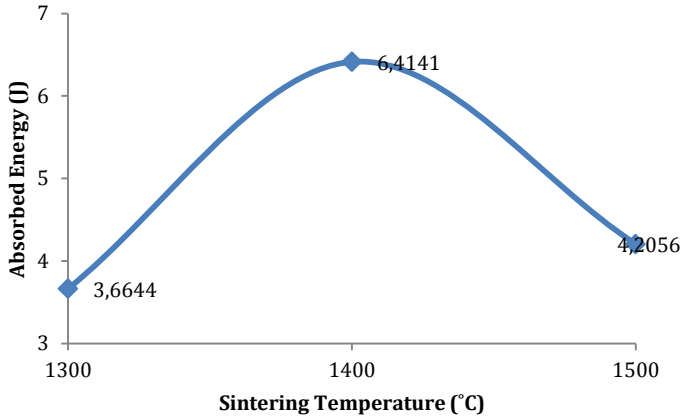

Fig. 7 Effects of Sintering Temperature on the Absorbed Energy of the Sample

According to Shaw, (1971) duringsintering process, the porosity of the ceramic body is reduced due to the vacancies and pores filling by molten (glassy phase). So, shrinkage size is equal to size of pore removed or lost. Sintering temperature has an extreme effect on the value of linear shrinkage as increasing sintering temperature leads to increases linear shrinkage due to increasing amount of molten filling pores and product high shrinkage in the sample. The limited expansion recorded makes the composite suitable for high temperature applications. According to Gupta, (2010), a refractory material should be able to maintain sufficient dimensional stability at high temperatures and after/during repeated thermal cycling.

3.2.2.8. Volumetric shrinkage (VS)

The effect of sintering temperature on the volumetric shrinkage (VS) is shown in Fig. 9. From the Figure, it is observed that the volumetric shrinkage of the sample sintered at 1300˚C is 7.0%, as the sintering temperature increased to 1400˚C the volumetric shrinkage slightly reduced to 5.32%, further increase in the sintering temperature to 1500˚C the volumetric shrinkage of the sample slightly increased in to 6.01%. This

followed the trend observed in linear expansion, but here the sample shrink slightly across the diameter, due to an increasing amount of mullite phase from kaolinite and increase quantity of cristobalite phase formed in the sample when the sintering temperature was raised from 1300˚C to 1500˚C. The high volumetric shrinkage observed at 1300˚C is due to quartz-cristobalite transformation, and the shrinkage reduces at 1400˚C, further increase in sintering temperature leads to slight increment at 1500˚C due to more liquid phase formation that fill the pore spaces. Amel, (2014) reported 5.3% as the minimum volumetric shrinkage recorded when Iraqi Red Kaolin was improved with the addition of silica and alumina. This implies that mullite-carbon ceramic composite produced has smaller shrinkage, which makes it to be better.

3.2.2.9. Oxidation Resistance

The effect of sintering temperature on the variation of oxidation resistance as depicted by oxidation index is shown in Table 3, Fig. 11 and Fig. 10. From the Figure, it is observed that with an increase in the sintering temperature, the oxidation index increased when the sintering temperature was raised from 1300˚C to 1500˚C. The oxidation index of the sample at 1300˚C is 0.225%, 0.43% at 1400˚C and 0.7395% at 1500˚C. It can be seen that the surface area around the cross section of

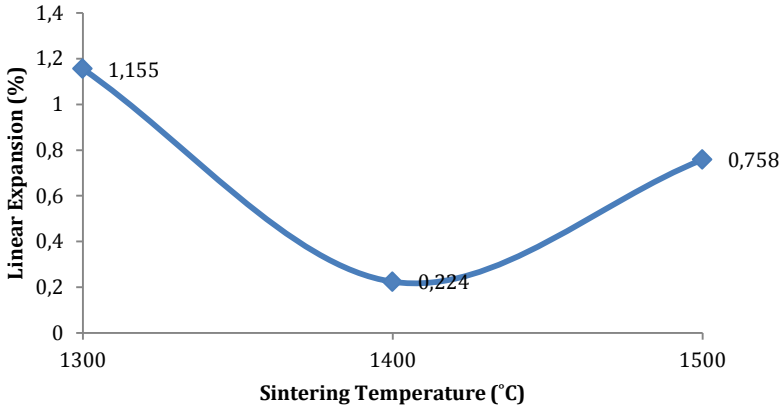

Fig. 8 Effects of Sintering Temperature on the Linear Expansion of the Sample

the samples showed clear variations in white contrast at various sintering temperature as a result of reaction between carbon and oxygen at high temperature shown in Fig. 10. A clear indication that the oxidation resistance reduces as sintering temperature increases. According to Zhang, (2004) the major drawback of carbon/graphite based refractories is that they are prone to oxidation at temperature above 900˚C. The limited oxidation of the composite produced at elevated temperature makes it suitable for high temperature application.

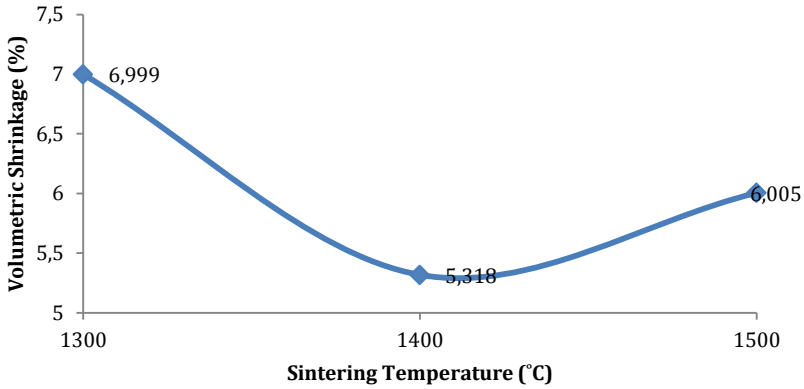

Fig. 9 Effects of Sintering Temperature on the Volumetric shrinkage of the Sample

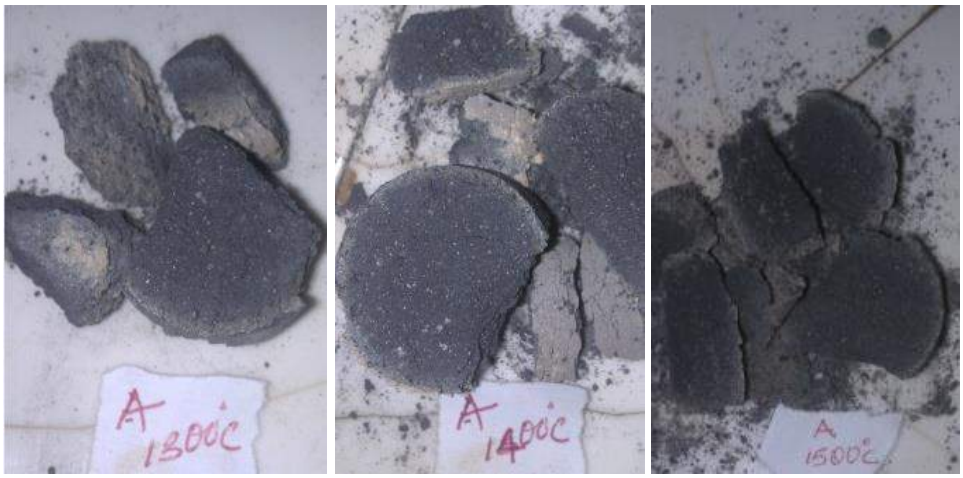

Fig. 10 Pictorial representation of Sectioned sintered Sample at varied Temperature.

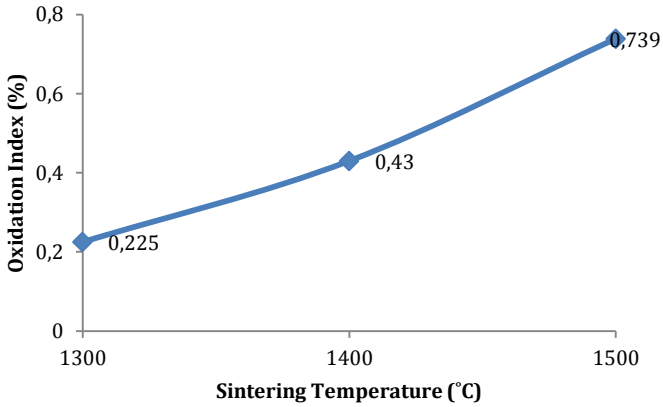

Fig. 11 Effects of Sintering Temperature on the Oxidation Index of the Sample.

Table 3
Physical and Mechanical Properties of the Sintered Sample

Temp. (°C)	Cold crushing strength (Mpa)	Modulus of Elasticity (Mpa)	Absorbed Energy (%)	Apparent Porosity (%)	Bulk Density (g/cm³)	Oxidation Index (%)	Linear Expansion (%)	Volumetric Shrinkage (%)
1300	7.23071	122.456	3.6644	29.513	1.596	0.225	1.155	6.999
1400	8.05027	141.280	6.4141	29.188	1.706	0.430	0.224	5.318
1500	7.00936	86.004	4.2056	29.926	1.472	0.739	0.758	6.005

4. Conclusion

From the discussion, it is concluded that;

- Due to high content of kaolinite phase, Okpella kaolin is suitable for the production of refractory and other ceramic applications at elevated temperature from its mineralogical composition;
- increase in sintering temperature leads to increase in the amounts of mullite and cristobalite phases produced within the ceramic composite samples;
- sample with optimum physico-mechanical properties is obtained at 1400°C

Acknowledgments

The authors acknowledge the Science Initiative Group (SIG), based at the Institute for Advanced Study in Princeton, for the support of this research work through the Competitive Fund for RISE Graduates Phase I (Round 1 and 3). Without this fund, it would have been extremely difficult to achieve the objectives of this research work.

References

1. Aksel C and Komicezny F. Mechanical properties and thermal shock behaviour of PSR333 alumina–mullite–zirconia refractory materials. Glass Int., 2001; 1: 16 – 18.
2. Aneziris CG, Klippel U, Schärfl W, Stein V, and Li YW. Functional refractory material design for advanced thermal shock performance due to titania additions. Int. J. Appl. Ceram. Technol., 2007; 4(6): 481 – 489.
3. Aneziris CG, Borzov D, and Ulbricht J. Magnesia-carbon bricks: a high-duty refractory material. Interceram Refractories Manual, 2003; 22-27: 119.
4. Aramide FO. Effects of sintering temperature on the phase developments and mechanical properties ifon clay. Leonardo Journal of Sciences, 2015; 26: 67 – 82.
5. Aramide FO, Alaneme KK, Olubambi PA, and Borode JO. Effects of 0.2Y-9.8ZrO2 addition on the mechanical properties and phase development of sintered ceramic produced from Ipetumodu clay. Faculty Engineering Hunedoara-International Journal of Engineering, 2014; 7(4), 343 – 352.
6. Aramide FO and Seidu SO. Production of refractory lining for diesel fired rotary furnace from locally sourced kaolin and potter's clay. Journal of Minerals and Materials Characterization and Engineering, 2013; 1: 75 – 79.
7. Aramide FO. Production and characterization of porous insulating fired bricks from ifon clay with varied sawdust admixture. Journal of Minerals and Materials Characterization and Engineering, 2012; 11: 970 - 975.
8. Badiee H, Ebadzadeh T and Golestani-Fard F. The effect of additives on mullitization of Iranian andalusite. 44th International Colloquium on Refractories, Achen, 126-130, 2001.
9. Benea M and Gorea M. Mineralogical and technological properties of some kaolin types used in the ceramic industry. Studia Universitatis Babes-Bolyan, Geologia, XLIX, 1, 33-39, 2014.
10. Brasileiro MI, Rodrigues AWB, Menezes RR, Neves GA and Santana LNL. Use of kaolin processing waste for the production of mullite bodies. Material Science Forum, 2012; 591-593: 117 – 143.
11. Brasileiro MI, Oliveira DHS, Lira HL, Santana LNL, Neves GA, Novaes AP, and Sasak JM. mullite preparation from kaolin residue. Material Science Forum, 2006; 530 – 531; 625 – 630.
12. Callister WD. Materials science and engineering: an introduction. 7th ed., John Wiley & Sons, Inc, 2007: 447.
13. Chandra D, Das GC, Sengupta U and Maitra S. Studies on the reaction sintered zirconia-mullite-alumina composites with titania as additive. Cerâmica, 2013; 59: 487 – 494.
14. Chen CY, Lan GS, and Tuan WH. Microstructural evolution of mullite during the sintering of kaolin powder compacts Ceramics International, 2000; 26: 715 – 720.
15. Das K and Banerjee G. Mechanical properties and microstructures of reaction sintered mullite-zirconia composites in the presence of an additive - dysprosia. Journal of the European Ceramic Society, 2000; 20 (2): 153 – 157.
16. Ebadzadeh T. Porous mullite-ZrO2 composites from reaction sintering of zircon and aluminum. Ceram. Int., 2005; 31: 1091 – 1095.
17. Ebadzadeh T and Ghasemi E. Effect of TiO2 addition on the stability of t-ZrO2 in mullite-ZrO2 composites prepared from various starting materials. Ceramics International, 2002; 28: 447 – 450.
18. Grim Shaw RW. The chemistry and physics of clays and allied ceramic materials, fourth edition. London, 1971.

19. Gualtieri AF. Thermal behavior of the raw materials forming porcelain stoneware mixtures by combined optical and in situ x-ray dilatometry J. Am Ceram Soc., 2007; 90: 1222 – 1231.
20. Gupta OP. Element of fuels, furnaces and refractories. Romesh Chander Khanna Publishers 2-B, Nath market, Nai Sarak Delhi India Fifth edition, 2010.
21. Hashimu H, Seungyong EP, Byung-Hyun C, Yong-Taie A, and Lee J. Influence of firing temperature on physical properties of Same clay and Pugu kaolin for ceramic tiles application. International Journal of Materials Science and Applications, 2014; 3 (5): 143 – 146.
22. Lee WE and Zhang S. Direct and indirect slag corrosion of oxide and oxide-c refractories. VII International Conference on Molten Slags Fluxes and Salts, The South African Institute of Mining and Metallurgy, 2004.
23. McConville CJ, and Lee WE. Microstructural development on firing illite and smectite clays compared with that in kaolinite. J. Am Ceram Soc., 2005; 88: 2267 – 2276.
24. Mahato S. Expanded graphite fortified magnesia-carbon refractories: fabrication and Properties. Master of Technology Thesis, Department of Ceramic Engineering National Institute of technology Rourkela, 2013; 11 – 24.
25. Merzah Amel S. Improvement of Iraqi red kaolin as a refractory. Material Eng. & Tech. Journal, 2014; 32, Part A, (4): 952 – 959.
26. Mesbah H, Wilson MA and Carter MA. The role of the kaolinite-mullite reaction sequence in moisture mass gain in fired kaolinite. CIMTEC Twelfth International Ceramic Congress, Part G, Montecatini Terme, Italy, 38 – 43, June 6–11, 2010.
27. Nabil RB and Barbara Z. Sample Preparation for atomic spectrometric analysis: an overview. Advances in Applied science research, 2012; 3 (3): 1733 – 1737.
28. Nemati Z, Sadrnezhaad S and Mooghari HRA. Effect of ferrosilicon, silicon and aluminum antioxidants on microstructure and mechanical properties of magnesia-graphite refractory. Refractories Applications & News, 2005; 10(6): 17-23.
29. Ozturk C, and Tur YK. Processing and mechanical properties of textured mullite/zirconia composites, J. Eu. Ceram. Soc. 2007; 27, 2-3: 1463-1467.
30. Qiu G, Jiang T, Li G, Fan X and Huang Z. Activation and removal of silicon in Kaolinite by Thermo-chemical process. Scan. J. Metallurgy, 2014; 33: 121 - 128.
31. Rendtorff NM, Garrido LB, and Aglietti EF. Thermal shock behavior of dense mullite–zirconia composites obtained by two processing routes. Ceram. Int. 2008; 34(8): 2017 – 2024.
32. Sadrnezhaad SK. Nemati ZA, Mahshid S, Hosseini S and Hashemi B. Effect of Al antioxidant on the rate of oxidation of carbon in MgO–C Refractory. Journal of the American Ceramic Society, 2007; 90 (2): 509 – 515.
33. Sadrnezhaad SK, Mahshid S, Hashemi B and Nemati ZA. Oxidation Mechanism of C In MgO–C Refractory Bricks. Journal of the American Ceramic Society, 2006; 89(4): 1308 – 1316.
34. Singh K. Specially treated graphite fortified alumina-silicon carbide-carbon refractories: fabrication and properties, Master of Technology Thesis, Department of Ceramic Engineering National Institute of technology Rourkela, 17 – 40, 2014.
35. Srikrishna K, Thomas G, Martinez R, Corral MP, Aza SD and Moya JS. Kaolinite-mullite reaction series: A TEM study. J. Mater. Sci., 1990; 25: 607 – 612.
36. Surappa MK. Aluminium Matrix Composites: Challenges and Opportunities; Sadhana, 28, Parts 1 & 2, 2003; 319 – 334.
37. Temoche F, Garrido LB and Aglietti EF. processing of mullite–zirconia grains for slip cast ceramics. Ceram. Int., 2005; 31, 917–22.

38. Tripathi HS, Das SK, Mukherjee B, Ghosh A, and Banerjee G. Effect of sillimanite beach Sand composition on mullitization and properties of Al2O3-SiO2 system. Ceram. Int., 2001; 27(8): 833 – 837.
39. Viswabaskaran V, Gnanam FD and Balasubramanian M. Mullitisation behaviour of Calcined clay-alumina mixtures, Ceramic International, 2003; 29: 561 – 571.
40. Zhang S. hydration behavior and antioxidizing effect of aluminium powder added to oxide-based castable. Proceeding of Tehran International Conference on Refractories, 2004; 75 – 79.